

# Development of thermoacoustic devices for power generation and refrigeration

Proc IMechE Part A:  
J Power and Energy  
227(7) 762–782  
© IMechE 2013  
Reprints and permissions:  
sagepub.co.uk/journalsPermissions.nav  
DOI: 10.1177/0957650913493622  
pia.sagepub.com



Artur J Jaworski and Xiaoan Mao

## Abstract

This paper is intended as a technical overview of the research and development work initially undertaken at the University of Manchester and subsequently transferred to the University of Leicester as part of the EPSRC-funded SCORE project (Stove for Cooking, Refrigeration and Electricity supply). The objectives of the work were twofold: Firstly, to develop an early demonstrator of a low-power electricity generator (to deliver approximately 10–20 W of electricity). This was to be based on the concept of using low-cost materials, working fluids and linear alternators suitable for deployment in rural areas of developing countries. The issues of concern here were the development of a suitable thermoacoustic engine topology and control measures; design of suitable heat exchanger configurations from initial use of electrical heaters to heat input through propane combustion; and characterisation of commercial loudspeakers to work as linear alternators and subsequent incorporation of selected models for engine prototyping purposes. These matters will be illustrated by a number of demonstrators and their testing in the laboratory environment. Secondly, to develop a demonstrator of a combustion driven thermoacoustic cooler for storage of vital medical supplies in remote and rural areas where there is no access to electricity grid. To this end, the paper will describe the design, construction and test results of an electrically driven demonstrator of a standing wave thermoacoustic engine coupled to a travelling wave thermoacoustic cooler. The final part of the paper will summarise the achievements to date and outline future work that has spun out from the original SCORE project. This will in particular include the current work on a scaled up version of electricity generator designed to deliver 100 W of electricity by using a two-stage engine configuration and the issues of integration of the thermoacoustic electricity generator and thermoacoustic cooler into one system.

## Keywords

Advanced power cycles, biomass, energy conversion/recovery, engine testing, heat exchangers, heat recovery, power from waste and biomass, power generation, shell/tube heat exchanges, Stirling engines, thermoacoustic refrigeration

Date received: 13 December 2012; accepted: 21 May 2013

## Introduction

Thermoacoustic technologies deal with the conversion between heat and acoustic power by relying on the so-called “thermoacoustic effect”. When a gas parcel undergoes the acoustic oscillations, it experiences a pressure change and a displacement from the equilibrium position. If the gas parcel is close to a solid material which possesses a temperature gradient, heat transfer could take place between the gas parcel and the adjacent solid material due to a local temperature difference. Hence, the appropriately phased pressure and displacement oscillations would enable the gas parcel to complete a useful thermodynamic cycle and thus to produce acoustic power by taking heat from the source at a higher temperature or to transport heat against the temperature gradient while consuming the acoustic power. These effects lead to two practical engineering implementations. One is to

impose an appreciable temperature gradient within the solid material. This results in the spontaneous generation of an acoustic wave along the direction of temperature gradient. Conversely, one could impose an acoustic wave in the compressible fluid, which would lead to hydrodynamic heat pumping effects along the solid material in the acoustic field. This results in the generation of a temperature gradient. These two interactions form the basis for engineering thermoacoustic engines and coolers (or heat pumps), respectively.

---

Department of Engineering, University of Leicester, Leicester, UK

### Corresponding author:

Artur J Jaworski, Department of Engineering, University of Leicester,  
University Road, Leicester, LE1 7RH, UK.  
Email: a.jaworski@le.ac.uk

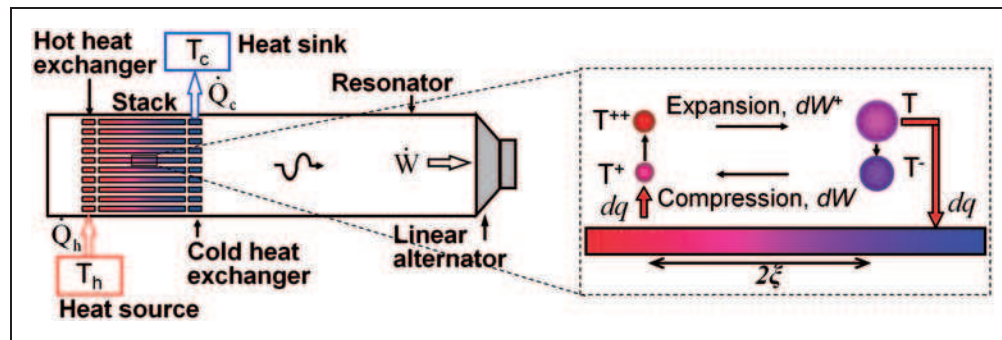


**Figure 1.** Simplified schematic drawing of a standing wave thermoacoustic engine.

In Figure 1, the schematic of a standing wave thermoacoustic engine is shown. A thermoacoustic stack put between hot and cold heat exchangers (HHX and CHX) is placed in the resonator. The gas-filled resonator is connected to a linear alternator at one end and has a solid wall at the other. When a sufficient temperature difference is applied along the stack, an acoustic oscillation starts spontaneously. A standing wave is present in a quarter-wavelength mode with the pressure anti-node at the solid wall end. The acoustic power transmitted along the resonator can be extracted by the linear alternator to provide electrical power. The gas parcels within the channels between stack plates undergo a thermodynamic cycle as shown on the right of Figure 1.

The thermoacoustic effect was qualitatively explained by Lord Rayleigh in 1878<sup>1</sup>: “If heat be given to the air at the moment of greatest condensation, or be taken from it at the moment of greatest rarefaction, the vibration is encouraged”. In 1960s, a quantitative theory was developed by Rott.<sup>2,3</sup> In his works, wave and energy equations were derived for the sound of a single frequency propagating along a channel possessing a temperature gradient.

The thermoacoustic engines can be generally categorized into two groups: standing-wave and travelling-wave, according to the phase difference between pressure and acoustic velocity oscillations. In the standing-wave engines,<sup>4,5</sup> the thermoacoustic core is often placed in a quarter- or half-wavelength resonator. The term “core” denotes an assembly of the stack sandwiched between HHX and CHX. Imperfect heat transfer between the gas and the solid material is realized to produce a significant time delay between the movement of the gas and its expansion (or contraction) to meet Rayleigh’s criterion. Due to this imperfect heat transfer, the thermodynamic cycle in the standing-wave engines is intrinsically irreversible and as a result they typically have relatively low efficiencies.

Ceperley<sup>6,7</sup> was the first to note the similarity between the thermodynamic cycle experienced by a gas parcel in a travelling-wave acoustic field and the Stirling cycle. The gas experiences expansion during the displacement toward the higher temperature and

contraction during the displacement toward the lower temperature, when the travelling wave propagates through the regenerator from its cold to hot end. Here, the solid material is referred to as a regenerator, following the convention in Stirling devices, to indicate that the thermal contact between the gas and the solid material is excellent. In this way, the correct time phasing is achieved to meet Rayleigh’s criterion, while efficiencies are significantly improved due to implementation of a reversible thermodynamic cycle. However, acoustic power is required to be fed into the cold end of the regenerator to exercise the Stirling-like thermodynamic process. Hence, the thermoacoustic core here resembles a power amplifier.

Thermoacoustic devices are thought to be particularly attractive due to the lack of moving mechanical components.<sup>4,8</sup> This provides a potential for high reliability and low maintenance. The working fluid is usually a pressurized noble/inert gas, making this technology environmentally friendly. Furthermore, for the thermoacoustic engine to operate, the required temperature difference can be relatively small. For example, de Blok reported that the acoustic oscillation starts at a temperature difference of only 65 K in the engine.<sup>9</sup> Therefore the thermoacoustic engine technology shows a great potential for utilizing waste heat, typically of low grade, or other renewable energy sources, such as biomass combustion and concentrated solar power.

SCORE (Stove for *Cooking, Refrigeration and Electricity* supply) is a £2 M research consortium, aiming to develop a stove which would contain the functionality of micro-generation of electricity and some cooling capability for remote and rural communities in developing countries. Both functionalities are to be provided by the development of appropriate thermoacoustic technologies. The SCORE partners are University of Leicester, University of Nottingham, Queen Mary University of London, City University London and a charity Practical Action. By its work, SCORE aims to significantly improve health and quality of life in the rural communities by understanding their energy needs and working with them in order to develop their capabilities to manufacture an affordable versatile

domestic appliance. The target device is to combine the functionalities of a high-efficiency cooking stove, an electricity generator and a refrigerator (cool box), which would be fuelled by burning biomass products. It is also conceivable to consider other renewable energy sources such as concentrated solar irradiation.

There is a clear need for developing the stoves described above: over 3.3 billion people live in rural areas; 2.4 billion people use biomass for cooking; about 2 billion people have no access to electricity, the great majority of them being rural people. The work is also going to ensure that in the long term the devices are acceptable at a technological, economic and social level and that there is a sufficient scope for the communities to develop numerous businesses from the manufacture, repair and innovative applications of SCORE. Naturally, such a complex project needs to be broken down into smaller tasks including: (i) social science studies, and in particular identifying the energy needs of the communities concerned<sup>10,11</sup>; (ii) design of the stove<sup>12</sup>; (iii) development of the thermoacoustic electricity generator; and (iv) development of the thermoacoustic refrigeration technologies. The final step will have to be the integration of various subsystems into one device.

Based on the social science research,<sup>10,11</sup> the current cost of a device, capable of producing 25 W peak electrical power for a family dwelling, is around 500 USD (275 GBP) – this is typically based on application of thermoelectric devices. However it is also clear that an acceptable price level is actually an order of magnitude lower: 50 USD (27.5 GBP) for a 25 W device, and of course proportionally more for higher powers. Social science research also indicates that the power rating of an ideal system for a rural dwelling in a developing country should aim at peak electrical power levels between 50 and 150 W, while the price should ideally be below 100 USD. Generating these amounts of electricity as a by-product of cooking activities (essentially bio-mass burning) would therefore be of immense benefit from the social perspective.

This paper is intended to provide an overview of the research and development work undertaken initially at the University of Manchester and subsequently at the University of Leicester for the SCORE project. Firstly, the developments of a number of demonstrators of an electricity generator to deliver 10–20 W of electricity are described. Issues of concern such as the engine topology, the heat exchanger configurations and the use of commercial loudspeakers as linear alternators are discussed. Secondly, the development of a demonstrator of a travelling wave cooler coupled with an electrically driven standing wave engine is presented. Towards the end, the paper will summarise the achievements to date and outline future work.

It should be mentioned that while this paper will not focus explicitly on the cost analysis of the proposed devices, and neither are the demonstrators

built to a specific cost, many of the design choices are driven by a “low-cost” approach which ultimately should be beneficial in the resulting mass produced devices. Good examples here are the choice of air at atmospheric pressure as the working fluid (to eliminate the need for expensive gases, unavailable in rural areas, and to allow using PVC pipes for resonators), devising uncomplicated heat exchanger topologies (to simplify manufacturing operations and thus reduce cost) or using loudspeakers as linear alternators. It will be helpful to the reader to bear this “low-cost” philosophy in mind while looking at the technical implementations and scientific context.

## Literature review

In the past decades, a variety of thermoacoustic engines have been devised to convert thermal energy to acoustic power using the thermoacoustic effect. Improvement of their thermal efficiency (i.e. from heat input to acoustic power output) remains one of the challenges. Swift<sup>4</sup> designed and tested a large scale standing-wave thermoacoustic engine. Pressurized helium was used as the working gas. The engine could deliver 630 W of acoustic power to the external acoustic load, converting heat into acoustic power at a thermal efficiency of 9%. Several other prototypes of standing-wave engines of different sizes or configurations have been studied by various researchers. The highest thermal efficiency, being the ratio of the acoustic power leaving the thermoacoustic core over the heat input, is reported to be only 18%.<sup>5</sup> The thermal efficiency of standing-wave engines is understood to have an upper limit of around 20%,<sup>8</sup> due to the already mentioned intrinsically irreversible thermodynamic cycle.

In order to overcome the efficiency limitations of standing-wave devices, travelling-wave devices became the focus of increased research interest. For instance, Sugita et al. used an electro-dynamic acoustic source to test the travelling wave power amplification for cryo-cooler applications.<sup>13</sup> Gardner and Swift designed a cascade thermoacoustic engine,<sup>14</sup> where one stage of a standing-wave thermoacoustic core is used to generate acoustic power to be fed into the adjacent travelling-wave stages for power amplification. Other various acoustic feedback mechanisms were used by Yazaki et al.,<sup>15</sup> de Blok,<sup>9</sup> and Backhaus and Swift.<sup>8,16</sup>

The above concept of a travelling-wave thermoacoustic engine was practically demonstrated by Yazaki et al.<sup>15</sup> A thermoacoustic core was placed in a one-wavelength looped-tube. Part of the acoustic power leaving from the hot end of the thermoacoustic core was transported back to the ambient end by the looped-tube. However, this engine was proved to have a very low efficiency due to, as realised later, the very low acoustic impedance in the regenerator, which

caused large viscous losses due to high acoustic velocities in the regenerator.

Subsequently, based on the concept of a compact acoustic network, Backhaus and Swift<sup>8,16</sup> designed a new type of thermoacoustic engine, which utilises high acoustic impedance to suppress the high acoustic loss. The thermoacoustic core was placed within a torus of a length much shorter than the acoustic wavelength. A long standing-wave resonator was connected to this torus just after the secondary ambient heat exchanger. Their thermoacoustic Stirling heat engine demonstrated a much higher thermal efficiency of 30%, which corresponds to 41% of Carnot efficiency. Essentially, the torus of the engine is an acoustic analogue of the free-piston Stirling engine by using a compact acoustic network which included acoustic inertance, compliance and resistance. In addition, a thermal buffer tube (TBT) and a “jet pump” were utilized to suppress the Rayleigh streaming and Gedeon streaming which cause the parasitical heat losses.<sup>8</sup> The long quarter-wavelength standing wave resonator was introduced to provide the acoustic resonance to allow the torus to work at a relatively low frequency, compared with the one-wavelength mode of the torus. For the same type of engine, a new record of 49% of Carnot efficiency has been more recently set by Tijani and Spoelstra.<sup>17</sup> A high temperature heat source was used at the engine hot heat exchanger (HHX), in order to produce a high temperature difference along the regenerator.

However, another separate and important challenge in the engineering of thermoacoustic engines is to reduce the temperature gradients required for the engine excitation. This is motivated by the utilisation of low grade heat. de Blok<sup>9</sup> pointed out that, in the torus-type travelling-wave engine, the combination of the high regenerator impedance and the large acoustic loss in the standing-wave resonator make the onset temperature difference, required for the engine excitation, very high. Therefore, he proposed a hybrid configuration with a travelling-wave feedback waveguide.<sup>9</sup> The designed travelling-wave thermoacoustic engine with a feedback pipe (FBP) could start at a temperature difference of only 65 K. Recently, a multi-stage version of this type of engine was able to start at a temperature difference of only 40 K at each stage.<sup>18</sup>

The acoustic power generated by the thermoacoustic engines from the heat input can be utilized in different ways. In general, it can be used for two main purposes: one is to directly convert the acoustic power to electricity through an electro-dynamic transduction mechanism; the other is to drive coolers or heat pumps,<sup>5</sup> which can be either thermoacoustic coolers (heat pumps) or pulsed-tube coolers.

Depending on the range of the acoustic impedance of electro-dynamic transducers, there may be different methods of coupling the transducers to the thermoacoustic engines. Several thermoacoustic generator

prototypes have been built and tested. A compact travelling-wave thermoacoustic generator prototype has been developed for electricity generation aboard spacecraft by integrating the thermoacoustic engine with a linear alternator.<sup>19</sup> Instead of using an acoustic resonator for the control of resonance frequency, the moving mass of the linear alternator is used as a reactive impedance to create a resonance with the compliant gas spring of the thermoacoustic Stirling engine volume. The device achieved a highest thermal to electric conversion efficiency of 18%. Alternatively, the linear alternator can also be coupled simply as a load to the standing-wave acoustic resonator of the thermoacoustic engine. In this case, the acoustic resonance remains to be provided by the acoustic resonator. A thermal to electric conversion efficiency of 15% was achieved in a recent work on this combination,<sup>20</sup> with the acoustic resonator dissipating an additional part of acoustic power. Other alternatives include integrating a piezoelectric generator with a thermoacoustic engine.<sup>21</sup>

In the aforementioned combinations of the thermoacoustic engines with the linear alternators, the linear alternators usually have very high acoustic impedance (i.e. large force and small displacement) at the operating frequency. They need to be installed at a high impedance region of the acoustic field in the thermoacoustic engines for optimal operation. The high impedance generally leads to a high pressure drop across the piston of the linear alternator. In most linear alternators, a clearance seal is usually adopted to avoid friction losses.<sup>19</sup> Therefore, when the pressure difference between two sides of the piston is high, the clearance seal could lead to high seal losses due to the gas passing through the gap, which constitute a form of acoustic streaming. Such streaming will accumulate the gas on one side of the piston and, as a result, the unequal mean pressure at two sides of the piston will create an excessive piston drift.

However, theoretically it is also possible to combine the thermoacoustic engines with low impedance (i.e. small force and large displacement) transducers. This combination has several advantages compared to its high impedance counterparts mentioned above. Firstly, installing such alternators in a low impedance region allows replacing the clearance seal with a “hermetic” seal which eliminates the seal loss and the possible piston drift in conventional linear alternators. Secondly, such a “hermetic” seal would also allow suppressing Gedeon streaming that usually exists within the looped-tube type of thermoacoustic systems. However, little research attention has been devoted to the combinations of the thermoacoustic engines with low impedance transducers. This is partly because there are no low impedance transducers readily available in the market, except the audio loudspeakers, which in turn are designed for high audio fidelity rather than the energy conversion purposes.

With all of above effects taken into account, the combination of a looped-tube travelling wave engine with low acoustic impedance transducers clearly has been considered as a viable development route for the SCORE project. Based on this concept, several demonstrators of the thermoacoustic electricity generators were developed and tested, and the main milestones are reported here.

The thermoacoustic refrigerators (and heat pumps) have also been a subject of significant research interest in the past decades, since Hofler demonstrated a successful prototype of a thermoacoustic refrigerator (cooler) driven by a loudspeaker.<sup>22</sup> Many thermoacoustic refrigerators have been developed and studied.<sup>23–25</sup> Specialised applications have also been investigated including gas liquefaction,<sup>26</sup> mixture separation<sup>27</sup> or a freezer for ice cream storage.<sup>28</sup> Since the early implementations of thermoacoustic refrigerators showed a relatively low performance, various parameters and components of the thermoacoustic refrigerators have been investigated for further improvement. These included the system configuration,<sup>29</sup> stack geometry,<sup>30,31</sup> working fluid,<sup>32</sup> the resonator,<sup>33</sup> the electrical driver<sup>34</sup> and other parameters.<sup>35</sup> The best cooling performance of a refrigerator achieved appears to be 30% of a coefficient of performance (COP) relative to Carnot COP for a cooling power of 210 W at 233 K.<sup>36</sup>

Thermoacoustic refrigerators can be driven by an acoustic driver such as a loudspeaker or linear compressor. They can also be driven by a thermoacoustic engine as the source of acoustic power. The coupling of thermoacoustic engine to a thermoacoustic refrigerator or pulse tube cooler has been investigated previously. One of the main foci was to obtain either a high performance systems or very low temperatures. Considerable research effort has been put into both simulation and experiment of such arrangements.<sup>37,38</sup> Devices of this type are capable of achieving the cryogenic temperature range,<sup>39,40</sup> down to about 2 K as reported by Wang et al.<sup>41</sup>

From a slightly different perspective, the complete system of a thermoacoustic engine driving the thermoacoustic refrigerator may be considered a “sustainable” system, if the heat source for the thermoacoustic engine is waste heat<sup>42,43</sup> or from renewable sources such as solar<sup>44</sup> or geothermal energy. There is a huge need of a cooler for storing vital medical supplies for the rural communities of developing countries. Since the electricity supplies may generally not be available, the cooling system driven by heat from a stove or renewable sources is particularly attractive.

The concept of a coaxial travelling wave cooler was firstly proposed and developed by Tijani and Spoelstra.<sup>45</sup> In the current work, the coaxial travelling thermoacoustic cooler is adopted and coupled with a standing wave thermoacoustic engine, which converts low grade energy (from biomass burning in a stove,

here simulated by electrical input) into acoustic power, which is in turn used to produce the refrigeration effect in the cooler. As already mentioned in the introduction, the design of such a target system has constraints on the capital cost, low maintenance and ease of repairs in the conditions where access to precision manufacturing and servicing facilities may be limited, but these will not attract significant attention in this paper.

## Thermoacoustic electricity generator

Currently, there are no linear alternators of low acoustic impedance readily available on the market. Therefore, in the current work, more conventional electro-magnetic transducers (i.e. easily available audio loudspeakers), were used as an approximation of the low impedance linear alternators. Their integration within the looped-tube type thermoacoustic engines leads to new challenges and design considerations. Here, the concepts of coupling audio loudspeakers to a thermoacoustic engine are investigated in detail, both theoretically and experimentally; generation of useful amounts of electricity is demonstrated.

### Concept and simplified model

The main concept of the thermoacoustic electricity generator based on the looped-tube configuration<sup>46</sup> is shown schematically in Figure 2. The thermoacoustic core consists of a CHX, a regenerator (REG) and a HHX. The acoustic power generated is partly extracted by the alternator (ALT), with the remaining part being returned to the cold end of the regenerator through the FBP for amplification. A sufficient temperature gradient in the direction of acoustic propagation is crucial for the regenerator to operate as an acoustic power amplifier, as it increases the volumetric velocity in the regenerator. With the acoustic pressure nearly constant, the acoustic power is thus increased. The regenerator has a much larger cross sectional area  $A$  than that of FBP, in order to improve the generator performance by having impedance  $Z \gg \rho_M a/A$ ,<sup>8</sup> where  $\rho_M$  and  $a$  are mean gas density and speed of sound, respectively. Two tapered sections are required to minimize the flow separations introduced and the corresponding streaming and heat leaks.<sup>47</sup> Flow straighteners can be installed to suppress streaming; these are indicated by dashed lines in Figure 2 and usually made of a few coarse mesh disks.

The TBT connects to HHX at one end and the secondary CHX (2<sup>nd</sup>CHX) at the other end to prevent a heat leak to the alternator housing. The alternator can be installed just after the 2<sup>nd</sup>CHX so that the acoustic power is extracted immediately after it is produced in the thermoacoustic core. An acoustic matching stub is introduced after the alternator, as shown in Figure 2. It is a simple side branch introduced to

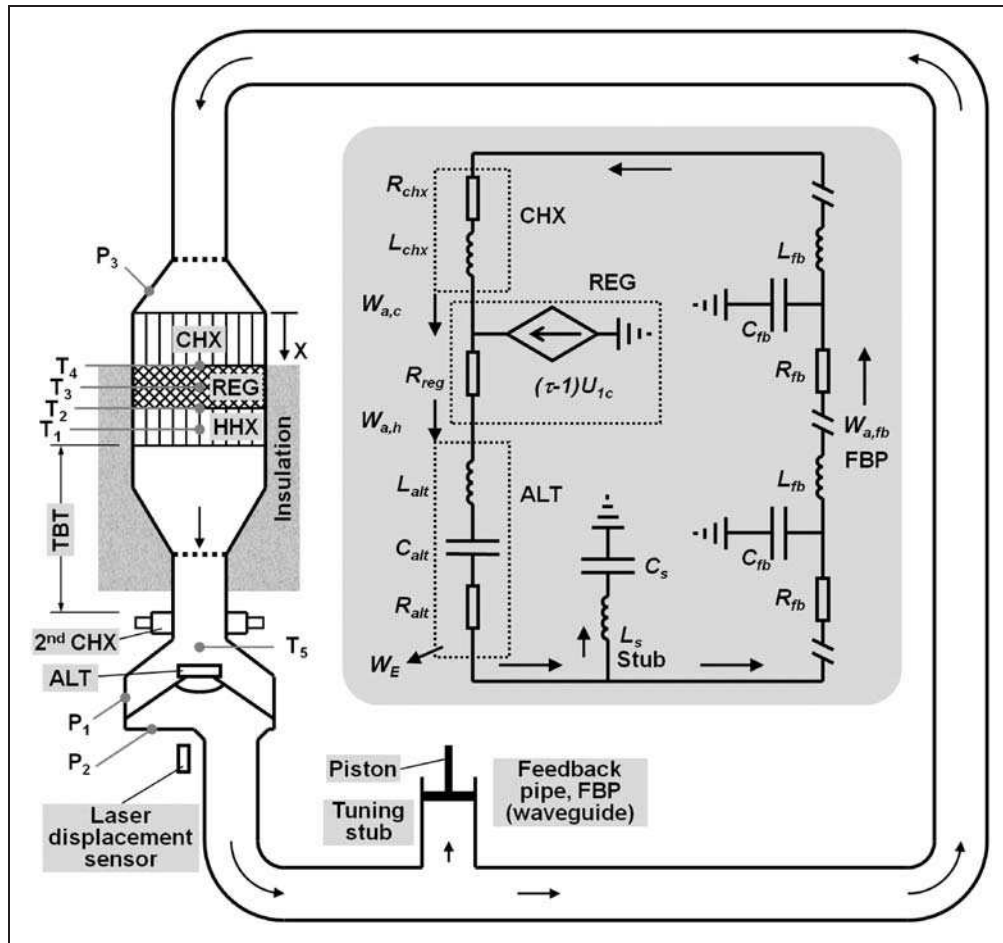


**Figure 2.** Schematic of the thermoacoustic electricity generator and the lumped electrical circuit.

cancel the acoustic reflection introduced by the alternator, by adding an equal and opposite reflection. The stub length can be varied by moving a piston placed in the pipe to enable a degree of fine tuning. Its effect on the engine performance is discussed in Section “Effect of stub on impedance matching”. After the stub, the long FBP connects back to the CHX.

According to the loudspeaker linear theory,<sup>48</sup> to achieve high transduction efficiency, the alternator should have a high force factor  $Bl$ , low mechanical resistance  $R_m$ , and low electrical resistance  $R_e$ . Furthermore, for a given frequency, the electrical power production capacity also depends on the excursion of the alternator; therefore, an alternator with a high excursion is preferred.

An equivalent lumped electrical circuit of the whole thermoacoustic electricity generator is also presented as an inset in Figure 2. This simplified model is very useful for understanding the behaviour of the system. However, the whole system is admittedly very complex by involving acoustic, mechanical and electrical components. Therefore, a more specialised modelling tool, referred to as Design Environment for Low-amplitude ThermoAcoustic Energy Conversion (DeltaEC), is employed for a quantitative analysis.<sup>49</sup>

### Construction and evaluation of the developed demonstrators

Over the project duration, several demonstrators were built and tested.<sup>46,50–52</sup> Each one had a different focus and has accordingly used different components or configurations to serve the purpose. In the following sections, the main features of each demonstrator are described and their performance, in terms of efficiency or power output, is presented and discussed.

**Demonstrator A.** The first demonstrator was driven by an electrical heater in order to have a good control of heat input for testing the system performance.<sup>50,51</sup> The overall layout is the same as shown in Figure 2. The main CHX is made out of a round aluminium block of 110 mm diameter and 90 mm length, as shown in Figure 3. Gas passages are made in the form of 45 holes of 5 mm diameter, parallel to the CHX centreline. Twelve holes of 6 mm diameter are made in perpendicular direction as passages for cooling water. The HHX is made in a similar way to the CHX, except that it is made out of brass to withstand much higher temperatures. It is 51 mm long and has 64 holes of 7 mm diameter parallel to the axis for gas passage. Nine ¼ inch holes are

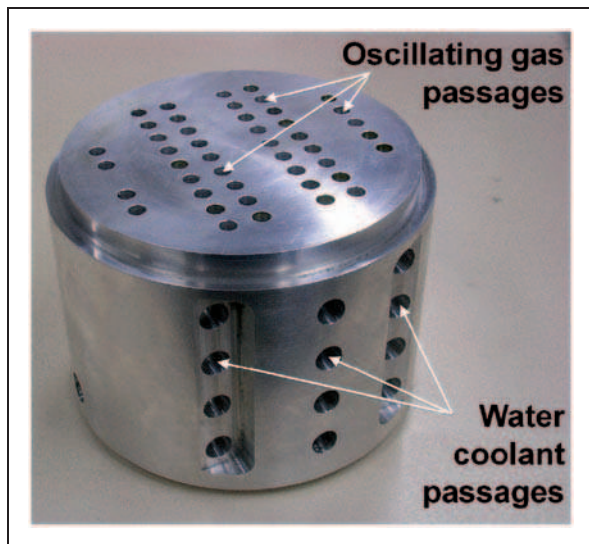


**Figure 3.** Cold heat exchanger used in demonstrator A. Here the water and gas flow channels are simply drilled in an aluminium block for ease of manufacture. Hot heat exchanger was made of brass due to higher temperatures used, but was conceptually of similar design.

prepared to hold nine cartridge heaters, each capable of providing 100 W of heat input. Thermocouples are embedded to monitor the temperature at various locations. The regenerator is made out of stainless mesh screen disks with the mesh number 34 and the wire diameter 0.254 mm. It has 33 mm length and is contained in a stainless steel regenerator holder, sandwiched between CHX and HHX.

Below the HHX there is a short section of a large diameter TBT, which is simply a section of stainless-steel pipe. The four parts described so far are clamped between two 4 inch flanges. To reduce heat losses, the regenerator, HHX and the short section of TBT are enclosed within a ceramic insulation material. The large diameter TBT is connected to a section of a smaller diameter TBT via a short transition cone, which reduces the diameter from 110 mm to 54 mm over a distance of 20 mm. A 2<sup>nd</sup>CHX is introduced to prevent the hot air reaching the alternator housing. The 2<sup>nd</sup>CHX is made out of a piece of car radiator that tightly fits inside the small-diameter buffer tube. A cooling water jacket surrounds the outside of the pipe at this position.

The alternator housing is installed about 50 mm below the 2<sup>nd</sup>CHX. A glass window is fitted in the bottom flange of the housing for a laser displacement sensor to measure the displacement of the alternator diaphragm. Pressure is measured before and after the alternator diaphragm. The FBP is made out of standard 2 inch PVC pipes and 90° elbows. The total length of the loop is 4.03 m which determines the operating frequency at 75 Hz with air at atmospheric pressure as working medium.

It should be noted that the CHX has a very low porosity of 10%. The gas passages are in form of

**Table 1.** Specifications of the loudspeakers used as alternators.

	B&C 6PS386	B&C 6PS386	B&C 8BG51	B&C 8BG51
	nominal	measured	nominal	measured
Nominal diameter (mm)	170	–	–	–
$F_s$ (Hz)	75	62	52	40.49
$Bl$ (T $\times$ m)	10.8	9.6	11.8	11.09
$L_e$ (mH)	0.6	0.479	0.5	0.48
$R_e$ ( $\Omega$ )	5.4	5.41	5.1	5.16
$Q_{es}$	0.31	–	–	–
$Q_{ms}$	11.7	–	–	–
$S$ (cm <sup>2</sup> )	132	–	220	–
$X_{max}$ (mm)	$\pm 6$	–	$\pm 6.5$	–
$M_m$ (g)	14	17.0	35	27.4
$K_m$ (N/m)	2778	2621	3736	1773
$R_m$ (kg/s)	0.64	0.96	0.93	1.23

5 mm holes of 90 mm length. As a result, the CHX produces a noticeable inertance effect in addition to the usual acoustic resistance.<sup>46</sup> This provides a phase change to help create the preferred condition for an efficient regenerator (i.e.  $U_I$  leads  $p_I$  at the cold end and  $U_I$  lags  $p_I$  at the hot end<sup>8</sup>). B&C 6PS38 loudspeaker is used as an alternator. Its specifications and the Thiele/Small parameters are summarized in Table 1. A high-power variable resistor is used as an electrical load for electrical power extraction. The alternator was installed after the TBT where the minimum of acoustic impedance appears in the loop. At this location, a sufficient volumetric velocity can be obtained to drive the alternator to a high excursion which should subsequently maximize the electrical power output.

When the alternator terminals are open, acoustic oscillation starts when the hot end temperature of the regenerator ( $T_1$ ) reaches 240 °C, with the cold end of the regenerator  $T_4$  always at 30 °C.<sup>51</sup> When a load resistor is connected, the temperature difference required for start up increases substantially. For instance, for a load resistance of 28.4  $\Omega$ , the acoustic oscillation starts when  $T_1$  reaches 261 °C. When the load resistance drops to zero (i.e. short circuit between the terminals), the onset temperature goes up to 530 °C.

Effects of heat input and load resistance on the generator performance were investigated.<sup>51</sup> The heat input was varied from 300 W to 800 W to change the temperature difference between the two ends of the regenerator ( $T_1$ – $T_4$ ), while the load resistance was fixed at 28.4  $\Omega$ . Generally, the acoustic power delivered to the alternator and absorbed by the alternator, and the electrical power extracted by the load resistor all increase linearly with the temperature difference ( $T_1$ – $T_4$ ), as shown in Figure 4a. At the highest input power of 800 W, the temperature difference across the

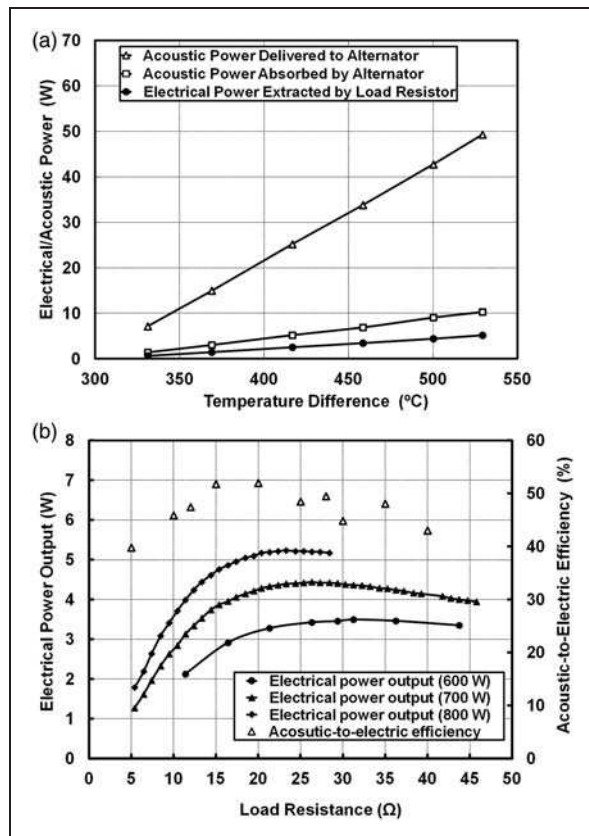


**Figure 4.** Performance characterisation of demonstrator A: measured acoustic and electrical powers versus the temperature difference between the two ends of the regenerator for load resistance of  $28.4 \Omega$  (a); electrical power output measured at three levels of heat input (left axis), and the acoustic-electric efficiency of alternator, when the heat input is  $700 \text{ W}$  (right axis), when different load resistance is applied (b).

regenerator is  $530^\circ\text{C}$ . The acoustic power produced that goes to the alternator is  $49.3 \text{ W}$  and the acoustic power absorbed by the alternator is  $10.3 \text{ W}$ . The load resistor extracts  $5.17 \text{ W}$  of electrical power. Here, the acoustic-to-electric efficiency,  $\eta_{A-E}$  is  $50\%$ , the thermal-to-acoustic efficiency, the ratio of the absorbed acoustic power over the heat input,  $\eta_{H-A}$  is  $1.29\%$ , and the thermal-to-electric efficiency, the ratio of the electrical power output to the heat input,  $\eta_{H-E}$  is  $0.65\%$ .

Effects of load resistance on the electrical power output from the alternator and  $\eta_{A-E}$  are shown in Figure 4b. The electrical power was measured at three heat input values. For a given heat input, there is an optimum load resistance that can extract a maximum electrical power. At the maximum heat input of  $800 \text{ W}$ , a maximum electrical power output of  $5.17 \text{ W}$  was obtained at the optimal load resistance of  $23 \Omega$ . For the heat input of  $700 \text{ W}$ , a maximum electrical power output of  $4.44 \text{ W}$  was obtained, at the load resistance of  $26 \Omega$ . The maximum  $\eta_{A-E}$  is  $52\%$  when the load resistance is around  $20 \Omega$ . The decrease in  $\eta_{A-E}$  at higher load resistances is considered to be related to the displacement of the loudspeaker

diaphragm. The experimental results show that the displacement of the diaphragm increases from  $2.0 \text{ mm}$  to  $5.1 \text{ mm}$ , when the load resistance changes from  $5 \Omega$  to  $40 \Omega$ . For this alternator, the maximum stroke is  $6 \text{ mm}$  (Table 1). The losses due to the non-linear effects would increase when the displacement approaches the maximum, and this may cause the reduction of  $\eta_{A-E}$ .

**Demonstrator B.** While demonstrator A was useful in showing that small amounts of electricity (just above  $5 \text{ W}$ ) can be generated, it was clear that there is a room for significant improvement. A weakness in the design proved to be the HHX. The brass block design was impractical – when clamped at elevated temperatures the HHX material deformed leading to problems with reliable seals. However on the thermal performance side it also proved unsatisfactory. The limited number of large diameter gas passages meant that not enough of thermal input from cartridge heaters was transferred to the working fluid, and this resulted in significant heat losses to the ambient. The changes incorporated in demonstrator B (Figure 5a) mainly addressed the improvement of solid-gas heat transfer in the HHX: Firstly, in place of the brass block, a thin cable heater ( $3.17 \text{ mm}$  diameter),  $2.4 \text{ m}$  long and rated at  $1000 \text{ W}$  was introduced. As shown in Figure 5b, it was wound into a spiral in two layers. Several coarse mesh disks were attached to enhance the heat transfer between the heater and working gas.

Further changes were introduced to the design of TBT, especially by changing the angle of contraction cone between large and small diameter TBT to reduce minor losses, but also by including the regenerator holder above the HHX as part of the TBT design (cf. Figure 5b). Further optimisation led to a shorter regenerator with  $21 \text{ mm}$  length. The stainless steel container, integrating functions of regenerator and HHX holder, and the TBT is surrounded by an insulation blanket (cf. Figure 5a). The total length of the loop is around  $4.25 \text{ m}$  which leads to an operating frequency of  $69\text{--}70 \text{ Hz}$  depending on the thermal condition.<sup>46</sup> The device starts acoustic oscillation at a lower temperature difference of  $120^\circ\text{C}$ . It can achieve a thermal-to-electric efficiency,  $\eta_{H-E}$  at  $1.4\%$  at its best, compared to  $0.65\%$  for demonstrator A. The maximum electrical power output is  $11.6 \text{ W}$  with a heat input of  $900 \text{ W}$ , the thermal-to-electric efficiency,  $\eta_{H-E}$  being  $1.3\%$ . It is worth noting that the changes introduced more than doubled the electrical output (from  $5.17$  to  $11.6 \text{ W}$ ).

The dependence of the electrical power output on the applied heat input is shown in Figure 6. Measurement results are indicated by the symbols, and the solid line shows the simulation results from DeltaEC. Both indicate that the electric power output increases with the heat input. At low power level, the prediction is close to the measured values. The



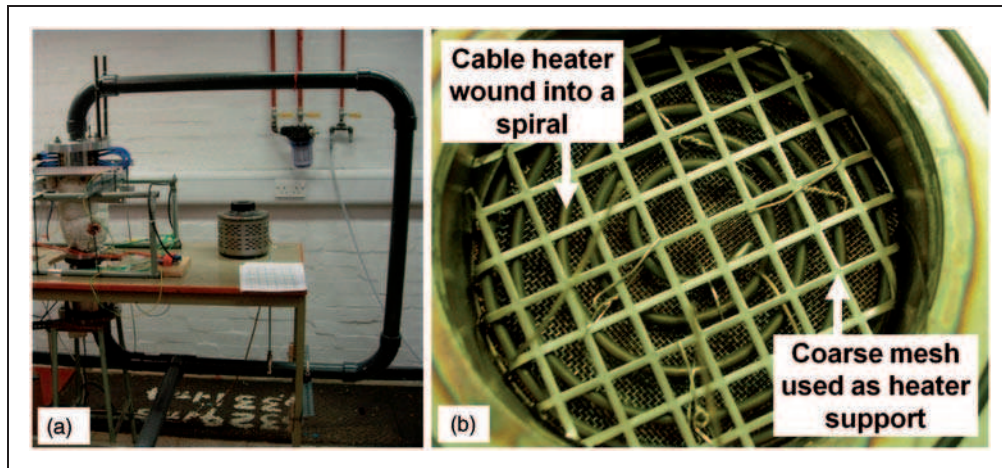


Figure 5. Photograph of the thermoacoustic electricity generator demonstrator B (a); and HHX assembly (b).

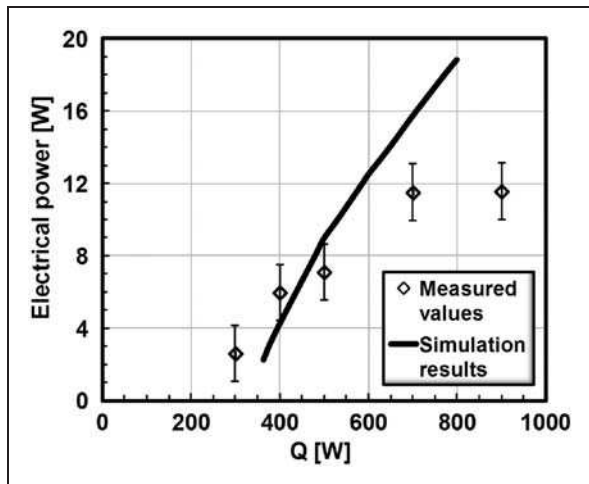


Figure 6. Electrical power output at various heat input levels. The load resistance is  $15.6 \Omega$ .

calculation overestimates the electrical power output at high power level. This could be mainly due to the fact that the heat loss to the ambient is considerably higher at a higher temperature. It is considered that the underestimation of the electrical power output when the heating power is less than 500 W is related to overestimated acoustic losses.

**Demonstrator C.** With a better understanding of the acoustic and thermodynamic behaviour of the combination of a looped-tube type engine with an alternator of low acoustic impedance, further effort was made to move one step closer to converting heat from combustion into electricity, by developing demonstrator C, as shown in Figure 7. The HHX was designed in a shell-and-tube configuration with working gas oscillating inside 37 stainless steel tubes, with internal diameter of 8 mm and 160 mm in length. The HHX porosity is about 19.6%. The thermal input is supplied by a propane gas burner with an adjustable heating power in

the range of 0–5 kW. The flue gas passes in between the tubes located in a chimney duct. The configuration of HHX has been chosen as a compromise between performance and ease of manufacture: welding a bundle of tubes should be easy to repeat in “blacksmithing” workshops in remote rural areas.

The space between the flange and the front face of the channels (cf. Figure 8) of the HHX accommodates the regenerator. It is 23 mm long and made from 72 stainless mesh screen disks. The same CHX is used as in previous demonstrators, albeit a wider angle cone was used to connect it to the PVC pipe in order to reduce minor losses. The TBT is part of the HHX design, in the form of a simple pipe extension at the back of the HHX. It is connected to a smaller diameter TBT via a short transition cone. A 2<sup>nd</sup>CHX is attached to the end of the TBT to remove residual heat. About 700 mm away from it, an acoustic stub is connected to the resonator to match the impedance between the alternator and the engine. The system performance was investigated with the alternator located at one of the pressure amplitude maxima, which is 965 mm away from the T-junction of the stub (Figure 7). This arrangement was designed to keep the influence of the alternator on the acoustic field in the engine to the minimum.<sup>52</sup> The total length of the loop is around 4.1 m, and the operating frequency is around 70 Hz.

When the alternator is not present, the acoustic oscillation starts when the temperature difference between two ends of the regenerator reaches  $107^\circ\text{C}$ . With the alternator installed and without any load resistance, a minimum onset temperature difference is  $134^\circ\text{C}$ . At the highest heat input, the solid temperature of the HHX reaches  $510^\circ\text{C}$ . The temperatures at the two ends of the regenerator are  $403^\circ\text{C}$  and  $112^\circ\text{C}$ , respectively. Electrical power of 8 W was extracted through the electrical resistor of  $15.8 \Omega$ , as indicated in Figure 9.

The electrical power output increases almost linearly with the temperature difference between the

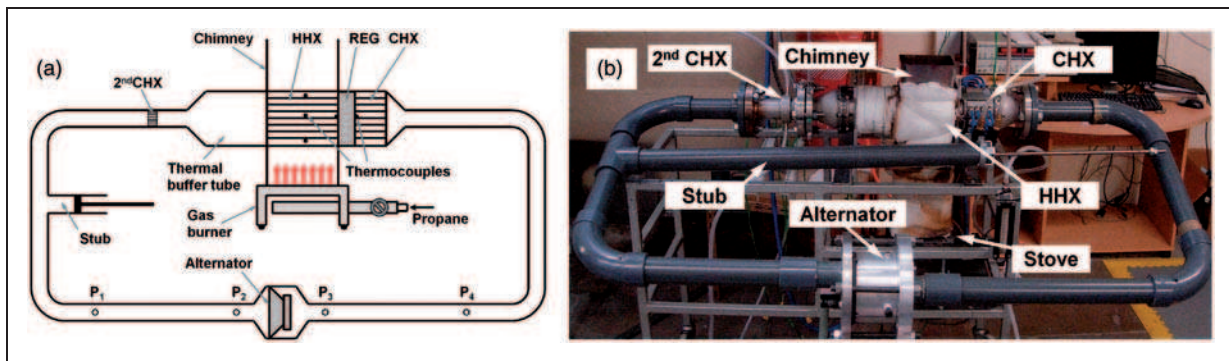


**Figure 7.** Schematic (a) and a photograph (b) of the thermoacoustic electricity generator demonstrator (C).

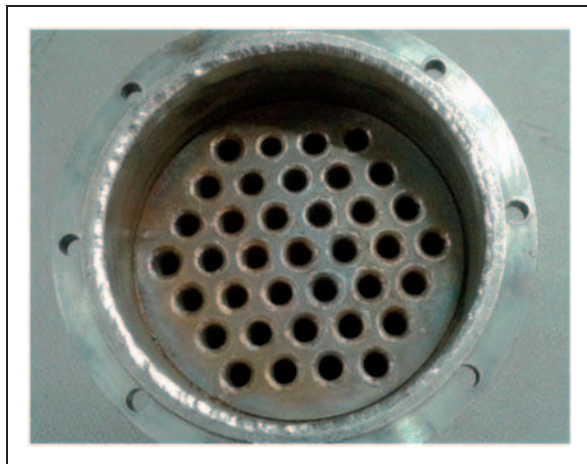


**Figure 8.** Front view of the shell-and-tube hot heat exchanger.

two ends of the regenerator. To protect the welding joints within the HHX, the solid temperature was limited to 500 °C, which meant that the temperature difference between two ends of the regenerator can only reach around 290 °C.<sup>52</sup> By a reasonable extrapolation, it would be possible to obtain around 15 W of electrical power if the temperature difference could be increased to 400 °C by exceeding the imposed solid temperature of 500 °C.

The acoustic-to-electric efficiency is around 35% according to the measured acoustic power with the two-microphone method.<sup>53</sup> In this configuration, the input heat from the gas burner and the net heat input to the engine were not measured. Thus, the overall thermal-to-electric efficiency is not available. A DeltaEC simulation was carried out to produce the pressure amplitude and the acoustic power flow along the loop, which are in good agreement with the measurements. According to the simulation,  $\eta_{A-E} = 53\%$ ,  $\eta_{H-A} = 4.6\%$  and,  $\eta_{H-E} = 2.4\%$ . However,  $\eta_{A-E}$  from measurement is considerably less than that from the simulation. This is thought to be linked to the acoustic losses that are caused by the sharp transitions between the FBP and alternator housing, which were not included in the DeltaEC simulations.

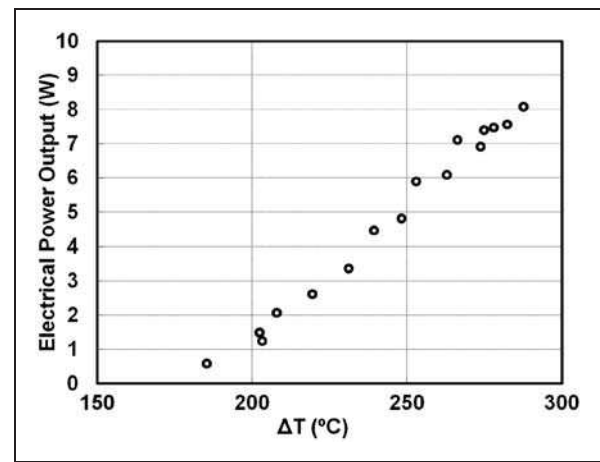


**Figure 9.** Electrical power output vs. temperature difference across the regenerator for demonstrator C.

**Demonstrator D.** One particular issue with demonstrator C was the limited temperature difference between the two ends of the regenerator, which prevents the engine from producing more acoustic power. It is constrained by the solid temperature of HHX (self-imposed experimental limit of around 500 °C) and a high cold end temperature of the regenerator, which could reach 112 °C. The latter is mainly caused by the design of the CHX, used in previous demonstrators, which does not have sufficient heat transfer area. Therefore, a first major change in demonstrator D was a new CHX, designed based on DeltaEC simulations. It is made out of an aluminium block with length of 60 mm. Gas passages are made in the form of 430 holes with the diameter of 3 mm, parallel to the CHX centreline, giving the porosity of about 32%. Passages for cooling water are made perpendicular to the CHX's centreline in a similar way as in the previous design. The regenerator, HHX, TBT and other parts of demonstrator C remain practically unchanged.

A second major change was in the configuration and type of the alternator used. It is connected through a 920 mm long pipe to the end of the TBT via a stainless steel T-junction (cf. Figure 10). Part of the acoustic power passing by the T-junction is extracted by the alternator; the remaining acoustic

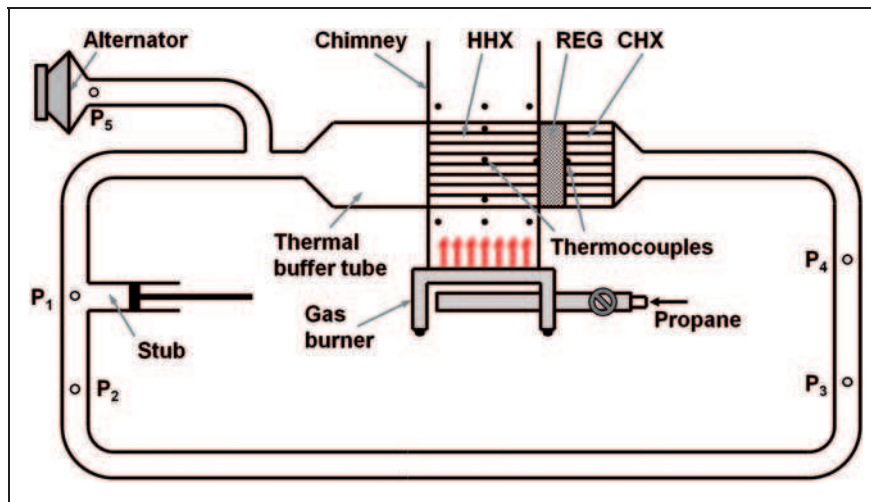


Figure 10. Schematic of the thermoacoustic generator demonstrator D.

power is transferred back to the thermoacoustic core along the FBP. Also, a different loudspeaker (B&C 8BG51) was utilized as the alternator for its relatively high transduction efficiency and low acoustic impedance (cf. Table 1). As in previous demonstrators, an impedance matching stub is adopted; the overall length of the loop is around 5.04 m, and the operating frequency is around 64 Hz.

A third major development compared to demonstrator C was that some quantitative measurements of heat input to the HHX were possible by enclosing the gas burner in a purpose built housing. The heat input to the HHX is worked out by measuring the inlet and outlet temperatures of the flue gas and its flow rate. The influence on the generation of electrical power due to the presence of the housing was also investigated by testing the demonstrator with and without the gas burner enclosed in the housing, as illustrated in Figure 11.

The demonstrator can produce 17.8 W of electrical power when the temperature difference across the regenerator reaches 340 K. When the gas burner is enclosed in the housing, the electrical power output is reduced. This is most likely related to different heat transfer characteristics of the HHX under two test conditions. Compressed air supply was used in the housing to force the flue gas through the tube bundle of the HHX, while the flue gas was driven by buoyancy only when the gas burner was not put in the housing. The resulting heat transfer and temperature distribution within the HHX would inevitably differ. The thermal-to-acoustic efficiency for this demonstrator is estimated to be around 3–3.5%, when the temperature difference was between 300 and 340 K. The efficiency decreases as the heat input decreases. The acoustic-to-electric efficiency decreases from 60 to 50%, as the displacement amplitude of the loudspeaker diaphragm increases. As a result, the thermal-to-electric efficiency was in a range of 1.5 to 2% for most of the test cases. The electrical power output of the

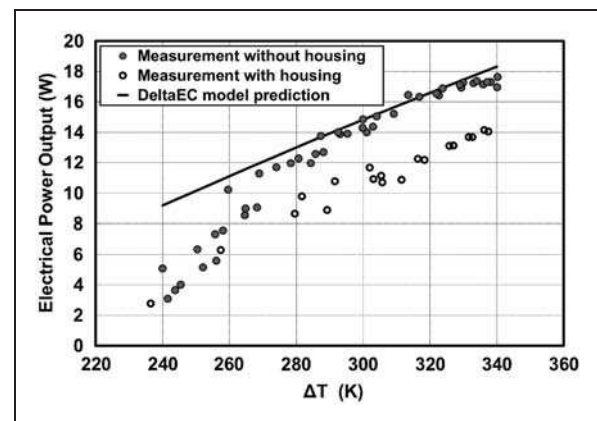
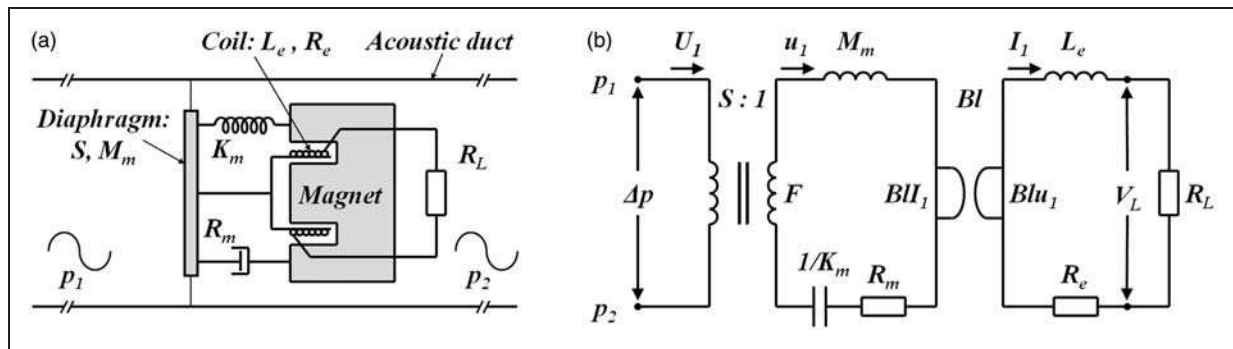


Figure 11. Electrical power output and temperature difference across the regenerator for demonstrator D.

demonstrator calculated from the DeltaEC model agrees well with the measurements when the gas burner is not included in the housing, as indicated by Figure 11. The discrepancy between the prediction and the measurement increases at smaller temperature difference across the regenerator. This is thought to be related to the temperature difference across the regenerator. Temperature measurements at a single point at the hot end of the regenerator were used to represent the mean temperatures in its cross section. The temperature in the cross section of the regenerator could be overestimated when  $\Delta T$  is small and the gas burner is not in the housing.

#### Characterization of audio loudspeakers as alternators

In principle, there are several commercially available transduction devices that can be used to convert acoustic to electrical power. These include commercial high impedance linear alternators (e.g. Q-drive type), piezoelectric transducers and the already mentioned audio



**Figure 12.** Schematic of the physics model of the loudspeaker (a) and its equivalent impedance circuit (b).

loudspeakers. The commercial high-impedance linear alternators often require precision manufacturing, while the piezoelectric transducers are very inefficient, and therefore these are not considered here. However, the ordinary audio loudspeakers are potentially good candidates for transduction devices used in SCORE, for two reasons. Firstly, they do not require precision manufacturing. Secondly, they can still achieve comparable power transduction efficiencies. However, they also have disadvantages such as a fragile paper cone and a limited stroke. Therefore, they are not suitable for high power applications, with a high pressure difference across the diaphragm. However, they may be suitable for relatively low power applications discussed in this paper, where the pressure difference across the diaphragm is usually in kPa range.

A simple linear model<sup>54</sup> of the loudspeaker that is used as a transduction device is developed and schematically shown in Figure 12. A pressure difference,  $\Delta p$  is applied on the loudspeaker diaphragm that has an effective area  $S$ , caused by the acoustic wave. The volumetric velocity due to the diaphragm displacement is  $U_1$ . The diaphragm and the coil, with a total mass,  $M_m$ , are subject to an oscillatory motion. The loudspeaker has a mechanical stiffness,  $K_m$ , and a mechanical resistance,  $R_m$ . The coil has an electrical inductance,  $L_e$ , and a electrical resistance,  $R_e$ . The force factor is  $Bl$ . A pure electrical resistance,  $R_L$  is connected as a load to extract electrical power in this model. The voltage on the load resistor is  $V_L$ , and the current is  $I_1$ .

In addition to the power extracted by the electrical load, part of the acoustic power absorbed by the loudspeaker is also dissipated by the mechanical resistance and the electrical resistance of the coil. For a loudspeaker, the electrical inductance of the coil is usually very small and can often be neglected. In order to extract the maximum electrical power by the load, its resistance,  $R_L$  should be equal to the electrical resistance of the coil,  $R_e$ . Maximum acoustic-to-electrical transduction efficiency is reached when the load resistance,  $R_L$  is equal to  $R_e\sqrt{1 + (BL)^2/R_mR_e}$ .

For a given candidate loudspeaker, its characteristics can be measured and investigated. Figure 13 shows the relationship between the measured

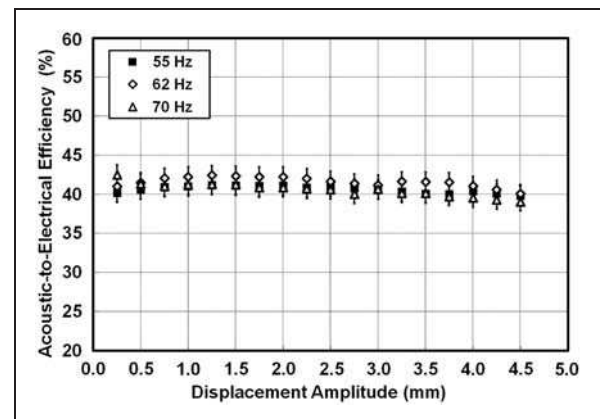


**Figure 13.** Acoustic-to-electric conversion efficiencies versus displacement amplitude plotted at different frequencies for the loudspeaker B&C 6PS38.

acoustic-to-electrical efficiency and the displacement of the diaphragm at three frequencies. The load resistance was fixed at  $5.57 \Omega$ , close to the coil resistance. The displacement amplitude was investigated in a range between 0.25 and 4.5 mm. It can be seen that the displacement amplitude does not affect the conversion efficiency significantly within the tested range. The efficiency increases and then decreases a little when the displacement amplitude increases from 0.25 to 4.5 mm. This implies that audio loudspeakers could be good candidates for alternators, when a high-displacement amplitude is required and a low-pressure drop is acceptable. The influence of load resistance on the acoustic-to-electrical efficiency was also studied with the displacement amplitude kept constant.<sup>54</sup> It is confirmed that an optimal load resistance exists, which leads to a high transduction efficiency. For the loudspeaker B&C 6PS38, an acoustic-to-electrical transduction efficiency of around 60% can be achieved. At the maximum power point, the transduction efficiency can still achieve 40%, as shown by Figure 13. Therefore, it is certainly practical to utilise the commercially available loudspeakers as alternators for such applications.

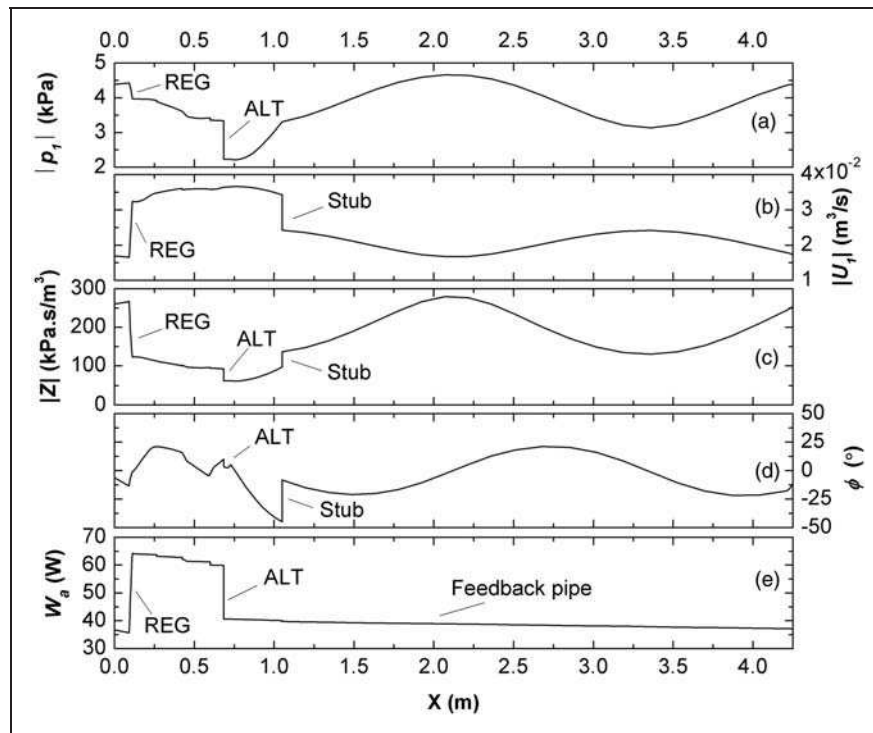


**Figure 14.** Pressure amplitude (a), volumetric velocity (b), acoustic impedance (c), phase angle (d) and acoustic power flow (e) along demonstrator B [Ref. 46, Copyright Elsevier].

### Effect of stub on impedance matching

In the current combination of a low-impedance alternator with the thermoacoustic engine, the alternator introduces an acoustic load to the thermoacoustic engine, which inevitably alters the acoustic field. An acoustically unmatched load generates an acoustic reflection and a high-standing wave ratio in the acoustic FBP and thus causes large acoustic losses. To extract the acoustic power in an efficient manner through the alternator and reduce the acoustic losses within the FBP, the load (alternator) has to match with the engine's acoustic network. This is achieved by applying a technique of "stub-matching", very similar to that routinely used in microwave electronic circuits. In practice, an acoustic stub is introduced and attached to the wave guide at a location close to the load. The characteristics of the matching stub and its effect on the acoustic field were carefully studied with demonstrator B.<sup>46</sup>

The pressure amplitude distribution along the 4.25 m long looped tube in demonstrator B is shown in Figure 14a. There are two maxima and two minima of pressure amplitude along the loop and two sharp pressure drops. One pressure drop is along the regenerator and the other at the alternator. Looking back to the simplified model as shown in Figure 2, the first pressure drop is caused by the flow resistance of the regenerator  $R_{reg}$ , while the second is caused by the acoustic resistance of the alternator,  $R_{alt}$ . The standing wave ratio within the loop can be estimated by the ratio of the maximum over minimum pressure

amplitude which is relatively small (about 2.1). The acoustic stub does not cause a change in pressure amplitude, while it changes the slope at which pressure amplitude increases.

The distribution of volumetric velocity along the loop is shown in Figure 14b. There are also two maxima and two minima along the loop. One maximum is in between the alternator and the stub, and the other near the end of the FBP where the minimum of the pressure amplitude is located. One minimum of the volumetric velocity is at the cold end of the regenerator, while the other is close to the middle of the FBP. At the location of the stub, there is a sudden decrease of the volumetric velocity, for the reason that the stub shunts part of the volumetric velocity away from the resonator.

Figure 14c shows the acoustic impedance along the loop. The acoustic impedance is highest at the cold end of the regenerator ( $Z \sim 5\rho_M a/A$ ). The impedance drops quickly because the pressure amplitude decreases while the volumetric velocity increases sharply from the cold to the hot end of the regenerator. The alternator causes a sudden drop of acoustic impedance due to the fact that the volumetric velocities at two sides of the alternator are the same, while the pressure amplitude drops significantly due to the power extraction. The stub essentially works as a Helmholtz resonator. It introduces a sudden increase of the acoustic impedance along the loop, by keeping the pressure amplitude constant and shunting part of the volumetric velocity. It is very clear that the stub cancels out (almost perfectly) the acoustic impedance

drop caused by the alternator. For an optimised performance, the stub should be close to the acoustic loads, which are the alternator and the acoustic resistance of the FBP in this case. After a careful simulation process, it has been located about 330 mm away from the alternator. From Figure 14c, it can also be found that  $0.6\rho_{Ma}/A < Z < 1.6\rho_{Ma}/A$  along the FBP. Therefore, the dissipation in the FBP has also been minimized.

The phase difference between pressure and velocity oscillation along the pipe is illustrated in Figure 14d. The regenerator is at a near travelling-wave location. The phase angle decreases rapidly after the alternator. The stub introduces a sharp increase of phase angle to counteract this sharp phase angle decrease.

The influence of the matching stub on the electrical power output can be seen more clearly from Figure 15. A comparison is made between the simulation and experiments when  $l_{\text{stub}}$  varies and  $R_L$  is fixed at  $15.6\ \Omega$ . In general, the measured  $\Delta p$  across the alternator has a good agreement with the

simulations. As  $l_{\text{stub}}$  increases,  $\Delta p$  increases significantly. In the experiments, as the stub length increases from 0 to 0.68 m, the extracted electric power  $W_e$  increases about ten-fold, which agrees with the simulation qualitatively (Figure 15b). Without the stub ( $l_{\text{stub}} = 0\ \text{m}$ ), the phase angle  $\phi$  is  $-71^\circ$  and  $61^\circ$  at the hot end of the regenerator and the beginning of FBP, respectively, while it approaches  $0^\circ$  when  $l_{\text{stub}} \approx 0.65\ \text{m}$  (Figure 15c). The design strategy is to achieve the near travelling-wave condition around the regenerator and within the FBP, so that the acoustic power production within the regenerator can be maximized, and the acoustic dissipation within the feedback loop is minimized. It is shown that the acoustic stub can effectively tune the phase to the preferred condition. This also explains the strong dependence of  $W_e$  on  $l_{\text{stub}}$ . The function of the acoustic stub has been frequently validated through the tests on the demonstrators being developed.

### Thermoacoustic refrigerator

Another important task of the project was the development of a thermoacoustic refrigerator. The objective of this task was to develop a demonstrator of a cooler for storing vital medical supplies for the rural communities of developing countries. Because the electricity supplies may generally not be available, it is thought that such a system could be driven by a thermoacoustic engine (powered by burning biomass) which delivers acoustic power to be utilized by a thermoacoustic refrigerator. In the current work, a standing wave thermoacoustic engine is chosen to convert the low grade heat from biomass burning in a stove, into acoustic power. The engine is coupled to a travelling wave thermoacoustic cooler, as shown in Figure 16. The cooler concept is similar to that developed by Tijani and Spoelstra,<sup>45</sup> namely a coaxial travelling wave configuration is adopted. Air at relatively low pressure of 10 bar is used as working medium. The linear configuration of Standing Wave engine (SWE) and Travelling Wave Cooler (TWC) would be beneficial for the ease of construction. From the literature discussed in section ‘‘Literature review’’, it is understood that there is generally lack of widely accepted ‘‘optimal’’ geometries for such SWE+TWC

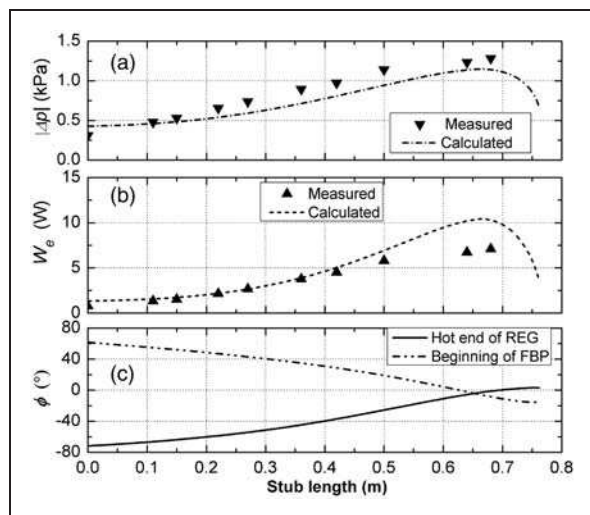


**Figure 15.** Comparison between the experiments and the simulation when  $l_{\text{stub}}$  varies: (a) pressure drop  $\Delta p$  across the alternator, (b) electric power extracted by the load resistor ( $R_L = 15.6\ \Omega$ ) and (c) the impact of the stub length on the phase angle in demonstrator B [Ref. 46, Copyright Elsevier].

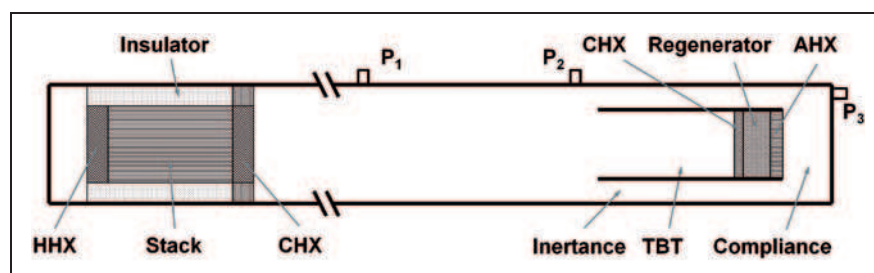


**Figure 16.** Schematic of the standing wave engine coupled with the travelling wave cooler.

couplings. This is because the optimal geometry strongly depends on the particular design targets and operating conditions and differs from case to case.

The main parts of the standing wave engine include: a stack, two heat exchangers and a resonator; their configurations are listed in Table 2. Electrical heating with Ni-Cr resistance heating wire was used within the HHX to provide heat input to the engine in order to simulate the biomass combustion at the current stage. The travelling wave cooler employs an acoustic network based on the same principle as the torus-shaped design<sup>45</sup> to create the travelling wave phasing necessary to operate the thermoacoustic Stirling cycle and help to create a high-acoustic impedance in the regenerator. The acoustic power produced by the engine is delivered to the cooler, where the acoustic waves move from the ambient side to the cold side through the regenerator in order to pump heat from the cold to the ambient side. The ambient heat exchanger is fixed at 288 K, which is the temperature of cooling water. A cooling temperature of 250 K at the CHX of the cooler was the design target.

In the design optimization of the travelling wave cooler, the configuration of the standing wave engine is fixed, as presented in Table 2. The design of the travelling wave cooler and its performance analysis were aided by DeltaEC. The optimization procedure was performed by varying the values of the parameters in each component, including the length and hydraulic radius of the regenerator, cooler diameter, length of the TBT and heat exchangers, and the compliance volume. The optimization process stops when the optimal configuration of the travelling wave cooler is achieved giving the maximum cooling performance indicated by the coefficient of performance

(COP). The COP is defined as the ratio of the heat load of the cooler,  $\dot{Q}_c$  and the acoustic power delivered to the cooler,  $\dot{W}_{ac}$  as follows

$$COP = \frac{\dot{Q}_c}{\dot{W}_{ac}}$$

The acoustic power delivered to the cooler is taken at a position just before the co-axial cooler from the output of the simulation.

As an example, the effects of the hydraulic radius and the regenerator length of the cooler on COP are illustrated in Figure 17. The ratio of hydraulic radius,  $r_h$  to thermal penetration depth,  $\delta_k$  is generally used in considering the regenerator geometry.<sup>55</sup> It can be

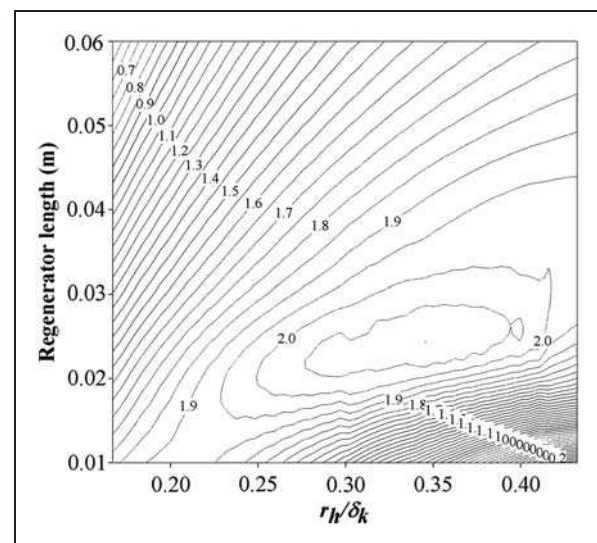


Figure 17. Contour plot of the effect of the regenerator length and ratio  $r_h/\delta_k$  on COP.

Table 2. Specification of physical components of the standing wave engine and the travelling wave cooler.

Part name	Dimensions	Other specifications
<b>The standing wave engine</b>		
Bounce space	211.58 mm ID, length 0.175 m	
Hot heat exchanger	40 mm length with same area as the stack (given below)	Resistance heating wire
Stack	Length 0.2 m Area $1.95 \times 10^{-2} \text{ m}^2$ Plate spacing 0.5 mm Plate thickness 0.2 mm Porosity 0.576	Parallel plate configuration of stainless steel
Cold heat exchanger	44 mm length with the same area as the stack	Water-cooled fin and tube heat exchanger
<b>The travelling wave cooler</b>		
Flow straightener	120 mm ID, length 0.75 mm	Stainless steel screens, mesh #20
Thermal buffer tube	120 mm ID, length 332 mm Wall thickness 1 mm	Thin wall stainless steel pipe
Cold heat exchanger	3.175 mm long with the same area as the regenerator	Coiled cable heater
Regenerator	110 mm ID, length 30 mm, $r_h = 3.7 \times 10^{-5} \text{ m}$	Stainless steel screens, mesh #160
Ambient heat exchanger	20 mm long with $8.17 \times 10^{-3} \text{ m}^2$ heat exchanger area	Fin and tube heat exchanger, mainly made of copper

regarded as an indicator of the effectiveness of thermal contact between gas and solid. If  $r_h/\delta_\kappa$  is low, a perfect thermal contact between working fluid and solid wall can be realized. However, this could increase the pressure drop across the regenerator considerably, which then results in low volume flow rate and causes low acoustic power transmitted to produce enough thermoacoustic refrigeration effect. The regenerator length has similar effects on COP. Generally speaking, a shorter regenerator causes smaller resistance to the flow, hence less consumption of useful acoustic power. However, the temperature difference created between the two ends of the regenerator is limited. If the regenerator is too long, the losses are much greater so that the cooling

performance deteriorates dramatically. Therefore, under these circumstances, the optimum regenerator length to utilize the acoustic power is obtained. The maximum COP obtained is approximately 2.06 at  $r_h/\delta_\kappa = 0.34$  and the regenerator length of 24.4 mm.

To compare the effects of individual parameters on the cooling performance, the dimensionless geometry ratio is introduced through normalisation by its optimal value as shown in Figure 18. The optimal geometry ratio equals unity at the maximum COP. Thus, this represents the sensitivity of COP to each parameter of the cooler. As can be seen, COP is extremely sensitive to the cross sectional area ratio of the FBP to resonator and the hydraulic radius of the regenerator, while much less sensitive to the length of the TBT. This implies that the cross section area of the regenerator and feedback/inertance tube, and the hydraulic radius of the regenerator are the vital parameters in the simulations of the coaxial thermoacoustic cooler driven by the thermoacoustic engine. At the optimal condition, the maximum achieved cooling load is 133 W at COP of 2.06.

According to the guidance given by the optimization procedure, as shown in Table 2, the standing wave engine and the travelling wave cooler have been constructed; selected photographs of the whole assembly and the individual components are shown in Figure 19. The operating frequency of the combined system is 46 Hz.

Sample experimental data from the cooler tests are presented in Figure 20. Figure 20a shows the evolution of the temperature of the cold end of the regenerator with time when 2.5 kW of thermal input is

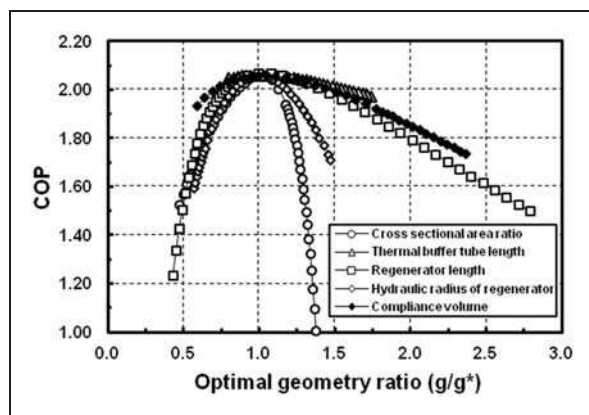


**Figure 18.** Variation of COP with dimensionless geometry of the travelling wave cooler.

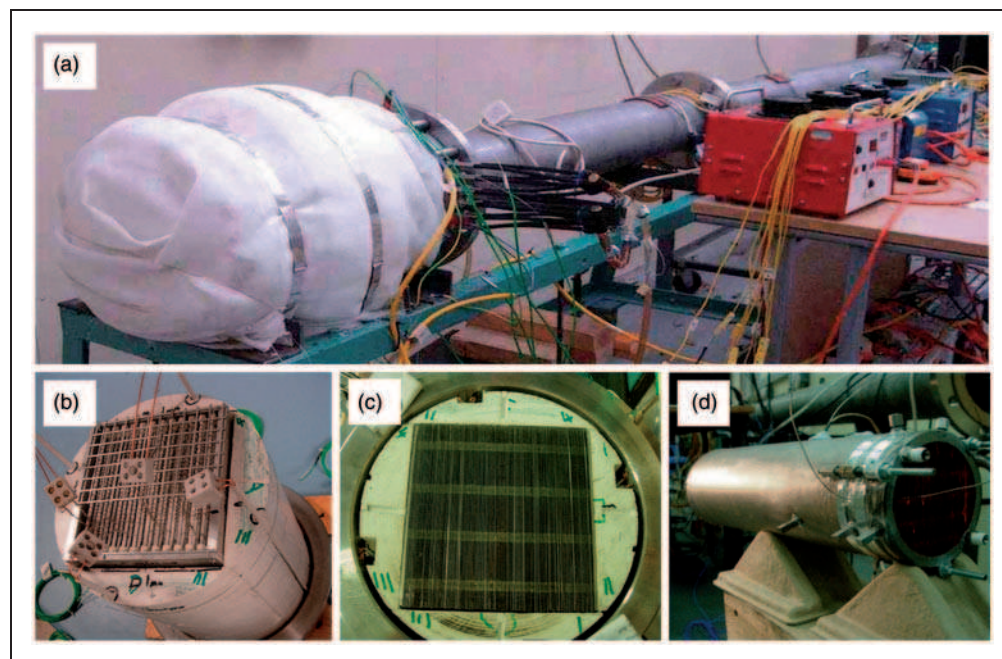


**Figure 19.** Practical implementation of the TWC driven by the SWE: overall view (a), the hot heat exchanger in SWE (b), parallel plate stack in the SWE (c) and the coaxial TWC cooler (d).



applied to the SWE (here 2.5 kW of heat input produces drive ratio of 3.25%). It can be seen that the temperature of around  $-18^{\circ}\text{C}$  is obtained after 30 min and around  $-20^{\circ}\text{C}$  after over an hour from the start of the test. Figure 20b shows the dependence of the minimum temperature obtained at the cold end of the regenerator as a function of drive ratio (obtained drive ratio values correspond to the heat input to the SWE). Finally Figure 20c shows the cooling performance in terms of COP against the applied cooling load for different values of drive ratio (i.e. heat input to the SWE). In the current study the cooling load is imposed by resistive heating. The acoustic power is calculated using the two-microphone method;<sup>53</sup> cf. sensors  $P_1$  and  $P_2$  in Figure 16.

### Current and future work

The development of and the relevant experiments carried out on several demonstrators described in previous sections illustrate the feasibility of developing electricity generators and refrigerators for rural communities based on the thermoacoustic technologies. However, there are several further steps that need to be taken in order to deliver systems that are relevant from the point of view of requirements of developing countries. Firstly, the electricity generator needs to be scaled up to deliver electric power in the range

of 100 W. In order to achieve this, a few challenges need to be addressed, including the application of a loudspeaker of a higher power rating, scaling-up the rig in the dimensional sense and adopting a concept of a two-stage engine design in order to better utilize the waste heat produced from cooking activities. Secondly, the target system should ideally include the functions of electricity generation and refrigeration in a single device (to operate simultaneously or in alternate fashion).

### Electricity generator based on two-stage thermoacoustic engine

As discussed previously, a looped tube travelling wave engine is relatively simple and easy to construct. It can also provide the travelling wave condition, where the alternator does not experience a high pressure difference across the diaphragm or piston. However, the electrical power output from the single stage thermoacoustic generator equipped with the second loudspeaker shown in Table 1 is limited to only about 18 W. In view of the limited length of the feedback loop (limited mainly by the resonance frequency of the loudspeakers) and the need to utilise a higher percentage of waste heat for a more efficient heat recovery process, one would ideally like to introduce a second stage of the engine. With this in mind, a

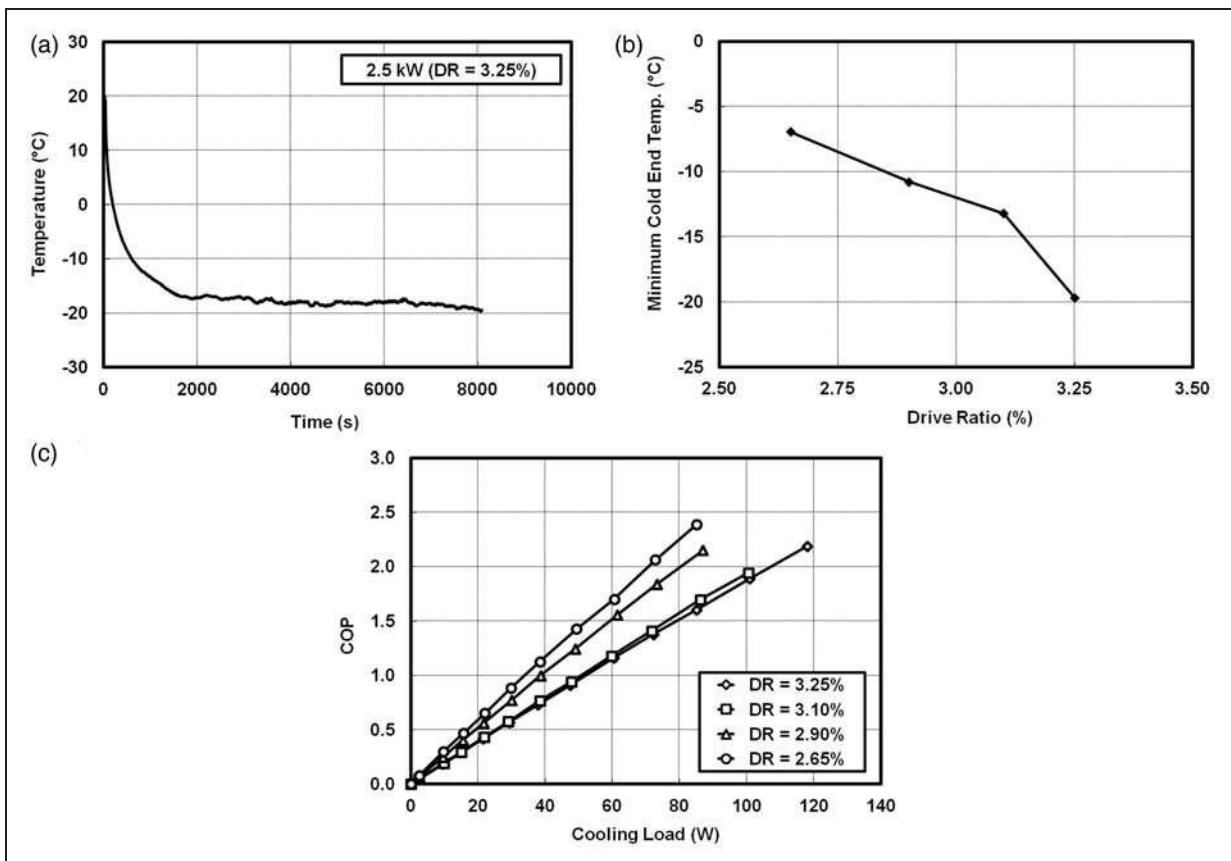
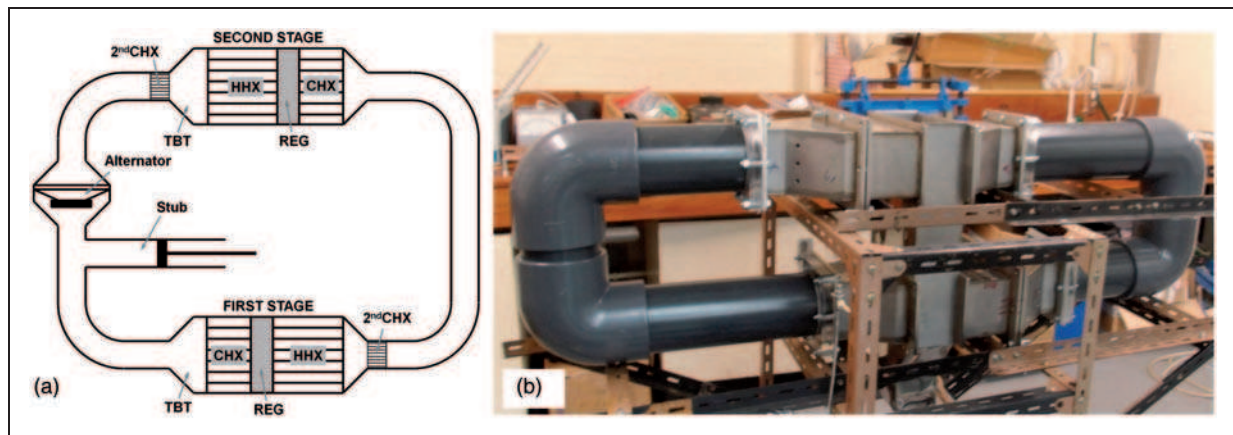


Figure 20. Selected data related to the cooling performance of the TWC.



**Figure 21.** Schematic (a) and early prototype (b) of the stage thermoacoustic electricity generator.

two-stage thermoacoustic engine has been designed and is being developed and tested in order to achieve a higher electrical output.<sup>56</sup> This arrangement has also the advantage of utilising low-grade heat source with a lower temperature difference across each stage.<sup>9,18</sup> The prototype uses air at two bar as the working gas and a commercially available high power woofer as an alternator. A schematic drawing of the prototype is shown in Figure 21a.

In the model, each stage consists of a regenerator made of stacked mesh screen discs, sandwiched between a parallel plate CHX and a shell-and-tube HHX, a TBT and a 2<sup>nd</sup>CHX. The two stages are connected through a FBP, with the alternator installed in between. The matching stub is connected to the looped engine in order to compensate the change of acoustic impedance due to the introduction of the alternator.

In an optimization process of the generator (similar to that undertaken for the thermoacoustic cooler presented in Section “Thermoacoustic refrigerator”), the effects of the porosity and length of HHXs, the length of regenerators, diameter of the FBP, and stub length have been investigated in order to find the optimal configuration. The objective was to achieve the highest electrical power output. The dimensions of CHXs/2<sup>nd</sup>CHXs are taken from the specifications of the commercially available car heater matrices. Heating power of 1 kW is applied at the HHX of each stage, although this may be an idealisation as the heat supplied to each of the two stages may not be equal. The stroke of the loudspeaker diaphragm is set to 8 mm, due to the limited excursion and a load resistance of 15  $\Omega$  is connected to the coil. The solid temperatures  $T_S$  of CHXs are set at the ambient temperature of 297 K.

The final model obtained after the optimization procedure gives a prototype operating at 96 Hz. The required heat input at two stages is 2136 W. Within the first and second stages, 159 W and 140 W of acoustic power are produced, respectively. The alternator extracts 210 W of acoustic power to produce 130 W of electricity. The calculated thermal-to-acoustic,

**Table 3.** Main parameters of the two stage thermoacoustic electricity generator.

Parameter	Value
Working frequency (Hz)	96
Working gas	Air
Mean pressure (bar)	2
Drive ratio/pressure amplitude (%)	6.1
Hot heat exchanger	Length (mm) 0.105
	Porosity 0.4288
	Plate spacing (mm) 8
	Heat input (W) 2136
	Solid temperature (K) 820
Regenerator	Length (mm) 30
	Porosity 0.82
Ambient heat exchanger	Length (mm) 49
	Porosity 0.62
	Size (mm <sup>2</sup> ) 235 $\times$ 129
Thermal buffer tube length (mm)	60
Stub length (mm)	820
Feedback pipe diameter (mm)	127

acoustic-to-electric, and thermal-to-electric efficiencies are 10%, 62% and 6%, respectively. The main parameters of the prototype are summarized in Table 3. Based on this, a demonstrator has been constructed, as shown in Figure 21b. Preliminary tests and debugging of the engine are currently underway and hence the prototype shown does not yet include all the envisaged components.

### *Thermoacoustic device combining electricity generator and cooler functionalities*

Another activity currently undertaken is the demonstration of the device which would enable combining the functionalities of an electricity generator and cooler in one configuration. Clearly, this was one of the original objectives of the SCORE project. One

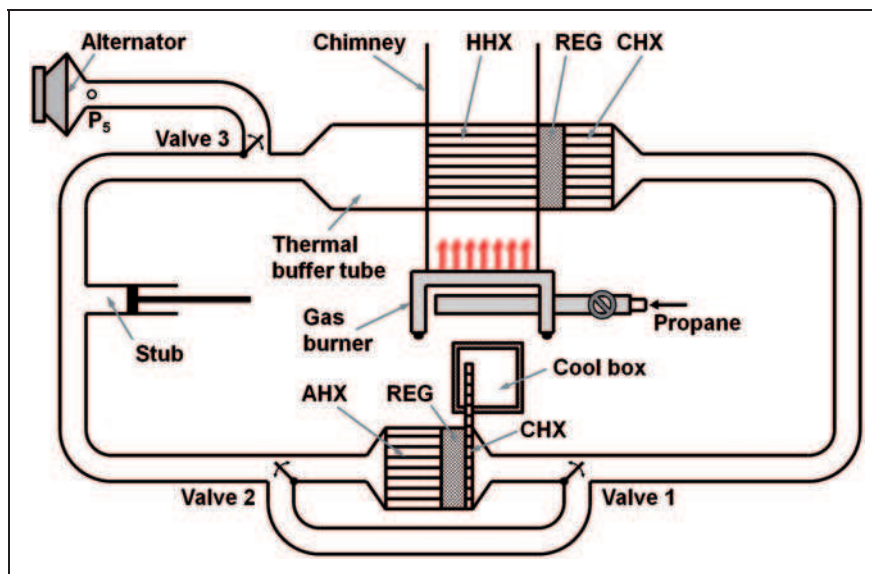


Figure 22. Possible configuration of the thermoacoustic device combining electricity generator and cooler.

of the simplest routes to obtaining such a device is to provide the alternative acoustic networks for an engine/generator and engine/cooler configuration enabled by opening/closing the flap/gate valves placed in the suitable places of the network. Figure 22 illustrates such configuration: by diverting the acoustic energy to the bypass duct by appropriate setting of flap valves 1 and 2 and opening the gate valve 3 to expose the alternator to the circulating acoustic power in the loop one could use the device as the electricity generator. On the other hand, by switching valves 1 and 2 to the position diverting the acoustic power flow through the cooler and shutting off gate valve 3, one could operate the device as a cooler. Clearly the lengths of the loop and bypass branch need to be selected in such a way that they correspond to the operating frequencies of the engine or cooler (they may not be the same). Similarly the tuning stub position may not be the same for the two alternative uses and may need to be adjusted appropriately.

### Closing remarks

This paper gives a technical overview of the research and development activities undertaken under SCORE project at the University of Leicester. Firstly, the process of developing a working prototype of the combustion-driven thermoacoustic electricity generator capable of achieving 18 W of electrical power output has been shown by illustrating the consecutive prototyping stages. The work described had to address many design issues including a suitable thermoacoustic engine topology and control measures; design of suitable heat exchanger configurations; and characterisation of commercial loudspeakers for incorporation in the systems under test as linear alternators.

Secondly, the presented work included a demonstrator of a thermoacoustic cooler for storage of vital medical supplies in remote and rural areas where there is no access to grid electricity. This has been driven by electrical heat input, but given the success of the combustion driven electricity generator it is only a matter of time to develop suitable heat exchangers for heat input from combustion processes. Further work is underway and this includes a two-stage engine to be used as an electricity generator capable of delivering around 100 W of electrical power and a combination of a cooler/generator functionalities to fulfil the main objectives of the SCORE project.

### Funding

Artur J Jaworski would like to acknowledge the support for his thermoacoustics research group received from EPSRC under grants EP/E044379/1 and EP/E044379/2.

### Acknowledgments

Both authors would like to acknowledge Mrs Patcharin Saechan and Mr Kalid Abdoulla (both are PhD students in the Thermoacoustic Technologies Group at the University of Leicester) for help with creating some of the illustrative material, while Dr ZB Yu is acknowledged for collecting data used in Figure 11. Dr HF Kang is gratefully acknowledged for developing the DeltaEC model of demonstrator D and subsequent generation of modelling data presented in Figure 11.

### References

1. Rayleigh L. The explanation of certain acoustical phenomena. *Nature* 1878; 18: 319–321.
2. Rott N. Damped and thermally driven acoustic oscillations in wide and narrow tubes. *Z Angew Math Phys* 1969; 20: 230–243.

3. Rott N. Thermally driven acoustic oscillations, part III: second-order heat flux. *Z Angew Math Phys* 1975; 26: 43–49.
4. Swift GW. Analysis and performance of a large thermoacoustic engine. *J Acoust Soc Am* 1992; 92: 1551–1563.
5. Wollan JJ, Swift GW, Backhaus S, et al. Development of a thermoacoustic natural gas liquefier. In: *Proceedings of AIChE meeting*, New Orleans, LA, 11–14 March 2002.
6. Ceperley PH. A piston-less Stirling engine – the travelling wave heat engine. *J Acoust Soc Am* 1979; 66: 1508–1513.
7. Ceperley PH. Gain and efficiency of a short travelling wave heat engine. *J Acoust Soc Am* 1985; 77: 1239–1244.
8. Backhaus S and Swift GW. A thermoacoustic-Stirling heat engine: detailed study. *J Acoust Soc Am* 2000; 107: 3148–3166.
9. de Blok CM. Low operating temperature integral thermoacoustic devices for solar cooling and waste heat recovery. In: *Acoustics'08*, Paris, 29 June–4 July 2008.
10. Sanchez T, Owala H and Okello V. Research into the behaviour of rural families to technology changes. In: *Proceedings of international conference on low-cost, electricity generating heat engines for rural areas*, Nottingham, UK, 2–3 April 2012.
11. Sanchez T, Dennis R and Pullen K. Cooking and lighting habits in rural Nepal and Uganda – SCORE Project. In: *Proceedings of international conference on low-cost, electricity generating heat engines for rural areas*, Nottingham, UK, 2–3 April 2012.
12. Dennis R and Pullen K. Development of wood-fired cooking stove to incorporate a thermo-acoustic engine-generator unit. In: *Proceedings of international conference on low-cost, electricity generating heat engines for rural areas*, Nottingham, UK, 2–3 April 2012.
13. Sugita H, Matsubar Y, Kushino A, et al. Experimental study on thermally actuated pressure wave generator for space cryocooler. *Cryogenics* 2004; 44: 431–437.
14. Gardner DL and Swift GW. A cascade thermoacoustic engine. *J Acoust Soc Am* 2003; 114: 1906–1919.
15. Yazaki T, Iwata A, Maekawa T, et al. Travelling wave thermoacoustic engine in a looped tube. *Phys Rev Lett* 1998; 81: 3128–3131.
16. Backhaus S and Swift GW. A thermoacoustic Stirling heat engine. *Nature* 1999; 399: 335–338.
17. Tijani MEH and Spoelstra S. A high performance thermoacoustic engine. *J Appl Phys* 2011; 110: 093519.
18. de Blok CM. Novel 4-stage travelling wave thermoacoustic power generator. In: *Proceedings of ASME 2010 3rd joint US-European Fluid Engineering Summer Meeting and 8th international conference on nanochannels, microchannels and minichannels, FEDSM2010-ICNMM2010*, Montreal, Canada, 2–4 August 2010.
19. Backhaus S, Tward E and Petach M. Travelling-wave thermoacoustic electric generator. *Appl Phys Lett* 2004; 85: 1085–1087.
20. Wu ZH, Man M and Luo EC. Experimental investigation of a 500W travelling wave thermoacoustic electricity generator. *Chin Sci Bull* 2011; 56: 1975–1977.
21. Jensen C and Raspet R. Thermoacoustic power conversion using a piezoelectric transducer. *J Acoust Soc Am* 2010; 128: 98–103.
22. Hofler TJ. *Thermoacoustic refrigeration design and performance*. PhD Thesis, Physics Department, University of California, San Diego, 1986.
23. Garrett SL, Adefe JA and Hofler TJ. Thermoacoustic refrigerator for space applications. *J Thermophys Heat Transfer* 1993; 7: 595–599.
24. Tijani MEH. *Loudspeaker-driven thermo-acoustic refrigeration*. PhD Thesis, Eindhoven University of Technology, Netherlands, 2001.
25. Ueda Y, Biwa T, Yasaki T, et al. Construction of thermoacoustic Stirling cooler. *Physica B* 2003; 329–333: 1600–1601.
26. Swift GW and Wollan JJ. Thermoacoustics for liquefaction of natural gas. *Gas TIPS* 2002; 8: 21–26.
27. Spoor PS and Swift GW. Thermoacoustic separation of a He-Ar mixture. *Phys Rev Lett* 2000; 85: 1646–1649.
28. Poese ME, Smith RWM, Garrett SL, et al. Thermoacoustic refrigeration for ice cream sales. In: *Proceedings of 6th IIR Gustav Lorentzen conference – natural working fluids*, Glasgow UK, 29 August–1 September 2004.
29. Yazaki T, Biwa T and Tominaga A. A pistonless Stirling cooler. *Appl Phys Lett* 2002; 80: 157–159.
30. Tijani MEH, Zeegers JCH and de Waele ATAM. The optimal stack spacing for thermoacoustic refrigeration. *J Acoust Soc Am* 2002; 112: 128–133.
31. Mao X, Saechan P and Jaworski AJ. Evaluation of random stack materials for use in thermoacoustic refrigerators. *ASME 2010 10th Biennial Conf Eng Syst Design Anal*, ESDA2010; 1: 229–234.
32. Tijani MEH, Zeegers JCH and de Waele ATAM. Prandtl number and thermoacoustic refrigerators. *J Acoust Soc Am* 2002; 112: 134–143.
33. Xie X, Li Q, Li Z, et al. Investigation on the different types of resonators in the thermoacoustic Stirling prime mover. *Ultrasonics* 2006; 44: e1503–e1505.
34. Paek I, Mongeau L, Braun JE, et al. Phase of acoustic impedance and performance of standing wave thermoacoustic coolers. *J Mech Sci Technol* 2009; 23: 1476–1484.
35. Shi L, Yu Z and Jaworski AJ. Vortex shedding flow patterns and their transitions in oscillatory flows past parallel-plate thermoacoustic stacks. *Exp Therm Fluid Sci* 2010; 34: 954–965.
36. Pierens M, Thermeau JP, Le Polles T, et al. Experimental characterization of a thermoacoustic travelling-wave refrigerator. In: *International conference on fluid mechanics, heat transfer and thermodynamics, (ICFMHTT 2011)*, Amsterdam, Netherlands, 13–15 July 2011.
37. Dai W, Luo E, Zhang Y, et al. Detailed study of a traveling wave thermoacoustic refrigerator driven by a traveling wave thermoacoustic engine. *J Acoust Soc Am* 2006; 19: 2686–2692.
38. Yu B, Luo EC, Li SF, et al. Experimental study of a thermoacoustically-driven traveling wave thermoacoustic refrigerator. *Cryogenics* 2011; 51: 49–54.
39. Dai W, Luo E, Hu J, et al. A heat-driven thermoacoustic cooler capable of reaching liquid nitrogen temperature. *Appl Phys Lett* 2005; 86: 224103.
40. Qiu LM, Sun DM, Yan WL, et al. Investigation on a thermoacoustically driven pulse tube cooler working at 80 K. *Cryogenics* 2005; 45: 380–385.
41. Wang C, Thummes G and Heiden C. A two-stage pulse tube cooler operating below 4 K. *Cryogenics* 1997; 37: 159–164.
42. Babaei H, Siddiqui K and Chishty WA. Sustainable thermoacoustic refrigeration system for gas turbine

- power plants. In: *17th symposium of industrial application of gas turbines (IGAT)*, Banff, Canada, 15–17 October 2007.
43. Gardner DL and Howard CQ. Waste-heat-driven thermoacoustic engine and refrigerator. In: *Proceedings of the annual conference of the Australian Acoustical Society: Acoustics 2009*, Adelaide, Australia, 23–25 November 2009.
  44. Adeff JA and Hofler TJ. Design and construction of a solar powered thermoacoustically driven thermoacoustic refrigerator. *J Acoust Soc Am* 2000; 107: 37–42.
  45. Tijani MEH and Spoelstra S. Study of a coaxial thermoacoustic-Stirling cooler. *Cryogenics* 2008; 48: 77–82.
  46. Yu Z, Jaworski AJ and Backhaus S. Travelling-wave thermoacoustic electricity generator using an ultra-compliant alternator for utilization of low-grade thermal energy. *Appl Energy* 2012; 99: 135–145.
  47. Gedeon D. DC gas flows in Stirling and pulse tube refrigerators. In: RG Ross (ed.) *Cryocoolers 9*. New York: Plenum, 1997, pp.385–392.
  48. Jordan EJ. *Loudspeakers*. London: Focal Press, 1963.
  49. Ward WC and Swift GW. Design environment for low-amplitude thermoacoustic engines. *J Acoust Soc Am* 1994; 95: 3671–3672.
  50. Yu Z, Backhaus S and Jaworski AJ. Design and testing of a travelling-wave looped-tube engine for low-cost electricity generators in remote and rural areas. In: *Proceeding of 7th international energy conversion engineering conference*, Denver, CO, USA, 2–5 August 2009, AIAA 2009-4540.
  51. Yu Z, Jaworski AJ and Backhaus S. A low-cost electricity generator for rural areas using a travelling-wave looped-tube thermoacoustic engine. *Proc IMechE, Part A: J Power and Energy* 2010; 224: 787–795.
  52. Yu Z and Jaworski AJ. Demonstrator of a combustion driven thermoacoustic electricity generator for remote and rural areas of developing countries. In: *Proceeding of the 19th international congress on sound and vibration*, Vilnius, Lithuania, 8–12 July 2012.
  53. Fusco AM, Ward WC and Swift GW. Two-sensor power measurements in lossy ducts. *J Acoust Soc Am* 1992; 91: 2229–2235.
  54. Yu Z, Saechan P and Jaworski AJ. A method of characterising performance of audio loudspeakers for linear alternator applications in low-cost thermoacoustic electricity generator. *Appl Acoust* 2011; 72: 260–267.
  55. Swift GW. *Thermoacoustics: a unifying perspective for some engines and refrigerators*. Sewickley, PA: Acoustical Society of America, Publications, 2002.
  56. Abdoulla KOA, Yu Z and Jaworski AJ. Design of a low-cost two-stage thermoacoustic electricity generator for rural communities in developing countries. In: *Proceedings of 19th international congress on sound and vibration*, Vilnius, Lithuania, 8–12 July 2012.